A Sequential Framework of Convolutional and Graph Convolutional Neural Networks: A Novel Technique For Lung Cancer Detection

*Mitul Goswami[1], Sainath Dey [1], Romit Chatterjee[1]
[1]School of Computer Engineering, Kalinga Institute of Industrial Technology, Bhubaneswar, 751024, India

* Corresponding Author

Abstract. This study significantly advances medical image processing and lung cancer detection through deep learning techniques and neural networks. The primary objective of this study is to accurately identify the presence of lung cancer and nodules within human lung image data. The research aims to enhance diagnostic accuracy by utilizing a comprehensive medical dataset comprising 15,000 histopathological images, divided into three classes—lung adenocarcinoma, lung squamous cell carcinoma, and benign lung tissue. The model effectively handles relational and spatial data by integrating Convolutional Neural Network (CNN) and Graph Convolutional Network (GCN) architectures, improving lung cancer detection capabilities. Comparative analyses with state-of-the-art studies demonstrate the superior performance of the proposed model, achieving an average accuracy of 97.80% across all three classes. The model's low loss value of 0.1326 underscores its proficiency in learning from training data. This comprehensive research underscores the intersection of medical sciences and machine learning, emphasizing the crucial role of precise image processing and synthesis in advancing diagnostic capabilities for complex medical conditions such as lung cancer.

Keywords: Lung Cancer Detection, Convolutional Neural Network, Graph Convolutional Network, Medical Image Processing, Histopathological Images

1 Introduction

Lung cancer, a leading cause of cancer-related mortality worldwide, has undergone significant evolution in our understanding, detection, and treatment over the years. Initially regarded primarily as a smoking-related disease, our comprehension of lung cancer has broadened to encompass various risk factors, including environmental pollutants, genetic predispositions, and lifestyle factors [1]. When lung cancer is diagnosed, it often signifies the presence of malignant growths within

the lungs, which can disrupt normal respiratory function. These tumors may obstruct airways, impair lung expansion, and interfere with gas exchange, leading to symptoms such as persistent cough, shortness of breath, chest pain, and coughing up blood [2]. Moreover, lung cancer can metastasize to other parts of the body, causing additional complications and further compromising overall health and quality of life. The development of advanced imaging technologies such as computed tomography (CT) scans has revolutionized early detection efforts, enabling the identification of suspicious nodules and lesions at earlier stages when treatment is more effective [3].

The evolution of technologies to detect lung cancer and other forms of cancer efficiently has been marked by remarkable advancements across various fronts. Early detection efforts have been revolutionized by imaging technologies such as computed tomography (CT) scans, magnetic resonance imaging (MRI), and positron emission tomography (PET), enabling the identification of cancerous lesions at earlier stages when treatment is more effective [4]. Furthermore, molecular profiling techniques, including next-generation sequencing and gene expression profiling, have provided insights into the genetic alterations driving cancer development and progression. These advancements have facilitated the development of targeted therapies and immunotherapies tailored to individual patients' molecular profiles, improving treatment outcomes and survival rates [5]. Additionally, the integration of artificial intelligence, particularly deep learning models like convolutional neural networks (CNNs) and graph convolutional neural networks (GCNs), has enhanced diagnostic accuracy and prognostic capabilities, leading to more efficient and precise cancer detection and management strategies [6].

Graph neural networks (GNNs) and graph convolutional networks (GCNs) offer promising avenues for efficiently detecting lung cancers by modeling the complex relationships within medical data. These networks can represent patient data as graphs, where nodes represent various medical features (e.g., imaging findings, genetic markers) and edges capture relationships (e.g., similarity, correlation) [7][8]. By leveraging this graph structure, GNNs and GCNs can effectively integrate heterogeneous data sources, including imaging data, patient history, and molecular profiles, to identify patterns indicative of lung cancer. This approach enables comprehensive analysis, enhances diagnostic accuracy, and facilitates personalized treatment strategies, ultimately contributing to more efficient and precise lung cancer detection and management [9]. The subsequent section delves into related studies, detailing the methodology and implementation of the proposed model. Subsequently, the discussion shifts to the outcomes observed.

2 Related Works

In recent years, advancements in the application of convolutional neural networks and other image-processing techniques, particularly deep learning and neural networks, have significantly enhanced the capabilities of lung cancer detection and other image-processing applications and use cases. The AlexNet Network Model with CNN layers was applied by [10]-[12] to identify lung tumors as benign or malignant. Similarly, [13]-[16] demonstrated an initial segmentation approach to segment out lung tissue from the rest of the CT scan using 3D CNNs for classification and detection. Subsequently, to detect lung cancer without imagery data, [17] [18] designed an Artificial Neural Network (ANN) based model that uses symptoms like yellow fingers, anxiety, chronic illness, fatigue, allergy, wheezing, coughing, shortness of breath, difficulty swallowing, and ensembles to determine if lung cancer is present in the human body or not. Further, [19] constructed individual lung graphs and divided the lung CT scans into ten segments to train a GCN model to forecast the 5-year overall survival. As a comparison, the existing TNM staging system, a convolutional neural network based on the tumor, a set of machine learning (ML) models, and a Cox proportional-hazard model were employed. Graph-based Variational Auto-encoder with a Gaussian mixture model and a GNN-based methodology were utilized by [20] and [21] respectively, to find relationships between sample patches to aggregate patch details into a unique vector representation that differentiates between lung squamous cell carcinoma (LUSC) and lung adenocarcinoma (LUAD), two subtypes of lung cancer and to investigate inhibitors in small cell lung cancer. [22] evaluated several deep neural networks to identify lung cancer. Compared to other algorithms in deep learning approaches, the research discovered that convolutional neural networks are employed for lung cancer diagnosis in many cases. In a different context, Fuzzy Clustering methods and algorithms were proposed by [23] [24] for sputum color picture segmentation to identify lung cancer in its early stages and for analyzing high-dimensional cancer databases. Subsequently, [25] introduced a multi-path CNN model that uses more global contextual variables in addition to local characteristics at the same time to automatically identify lung cancer. To this purpose, the model employs three routes, the receptive field sizes of each of which vary, aiding in the modeling of distant dependencies (both the short- and long-range dependencies of the neighboring pixels.

In contrast to contemporary methods that predominantly focus on individual implementations of either convolutional neural networks (CNNs) or artificial neural networks (ANNs), our proposed model stands out by integrating both CNNs and graph convolutional networks (GCNs). This innovative approach synergizes the strengths of CNNs in extracting features from medical imaging data with the graph-based representation offered by GCNs. GCNs excel in handling spatial data by leveraging the inherent graph structure of lung cancer images. By modeling

relationships between image regions as nodes and their spatial connections as edges, GCNs effectively capture spatial dependencies and contextual information within the image, enabling more comprehensive analysis and precise localization of cancerous lesions. This integration of CNNs and GCNs thus presents a holistic solution for accurate and efficient lung cancer detection.

3 Methodology

In this study, the authors have integrated layers of CNNs with GCNs, concatenating them after flattening to achieve results. The following section elaborates on the specific methodologies utilized for the experimentation. Fig. 1 gives the visual representation of the architecture of the proposed CNN-GCN model.

3.1 Data Normalization and Preprocessing

Initially, the distribution of classes within the dataset is analyzed using value_counts() to understand the data balance. After the initial phase, the dataset undergoes a meticulous partitioning process facilitated by the train_test_split function. This pivotal step ensures that the dataset is appropriately divided into distinct subsets tailored for different stages of the machine learning pipeline. Specifically, the training set is allocated 80% of the data, serving as the cornerstone for model training and parameter optimization. Meanwhile, the remaining 20% of the dataset is evenly split between the validation and testing sets. This balanced distribution ensures that each subset captures a representative sample of the overall data distribution, mitigating the risk of overfitting and enabling robust model evaluation. By delineating distinct subsets for training, validation, and testing, the data preparation phase lays a solid foundation for subsequent model development and performance assessment. Image data preprocessing is facilitated using the ImageDataGenerator class from Keras, which allows for real-time data augmentation and normalization.

$$X_{norm} = \frac{X_{orig} - \mu}{\sigma} \tag{1}$$

In equation (1), X_{norm} represents the normalized pixel value, X_{orig} represents the original pixel value, μ is the mean of the pixel values across the dataset and σ is the standard deviation of the pixel values across the dataset. This formula is applied to each pixel of the image to scale its intensity to a standard range, typically [0, 1] or [-1, 1], by subtracting the mean and dividing by the standard deviation. Normalizing pixel values helps reduce the effect of varying pixel intensity ranges across different images, making the training process more stable and efficient. The flow_from_dataframe method is utilized to generate batches of image data from the dataframe, where images are resized to a specified target size, normalized, and converted into RGB format. These batches of preprocessed image data are then utilized for training, validation, and testing of the machine learning model.

$$Resized\ Image = Original\ Image \times \frac{NW}{OW} \times \frac{NH}{OH} \quad (2)$$

In equation (2), the *Resized Image* is the image after resizing, *Original Image* is the input image. *NW* and *OW* represent the New Width and Original Width respectively. Similarly, *NH* and *OH* represent the New Height and Original Height. resizes the image by interpolating pixel values to fit the specified dimensions while preserving the aspect ratio of the original image.

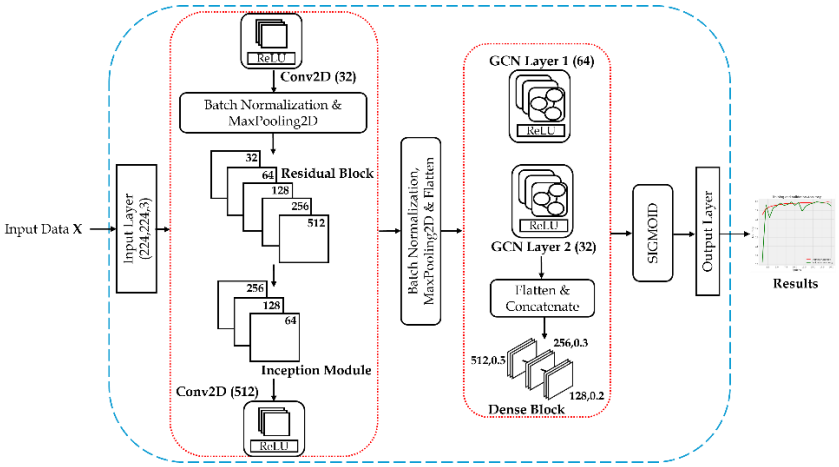

Fig. 1. Architecture of the Proposed CNN-GCN Model

Resizing is a crucial preprocessing step to ensure that all images in the dataset have consistent dimensions, facilitating uniform processing and analysis by the machine learning model. Finally, sample images from the training set are visualized to gain insights into the data and verify the correctness of the preprocessing steps. This visualization aids in confirming that images are correctly loaded, resized, and labeled, providing a crucial quality check before proceeding with model training.

3.2 Model Architecture

Input Layer

The input layer serves as the model's entry point, receiving image data with dimensions (224, 224, 3), where 224x224 represents the spatial resolution and 3 signifies the three RGB color channels. These dimensions are crucial for understanding the structure of the input data and are fundamental for subsequent processing steps.

Convolutional Layer

Convolutional layers are pivotal components in the model, responsible for extracting hierarchical visual features from input images. These layers apply learnable filters, or kernels, through convolution operations across the image's spatial dimensions.

The convolution operation involves element-wise multiplication of filter weights with local regions of the input tensor, followed by bias addition. Mathematically, this is represented as the dot product of the filter weights and the input tensor, summed with a bias term. The convolution process allows the model to detect low-level features, such as edges and textures, in the initial layers, and then progressively learn more complex and abstract features in the deeper layers. In equation (3) Let X represent the input tensor to the convolutional layer, W denote the convolutional kernel (filter) weights, and b represent the bias term. The convolutional operation is defined as the element-wise multiplication of the filter weights W with a local region of the input tensor X, followed by summation and addition of the bias term b, where $Z_{i,j}$ is the output value at position (i,j) in the output feature map, $X_{i+m,j+n}$ represents the input value at position $(i+m,j+n)$ in the input tensor, and M and N are the dimensions of the convolutional kernel W.

$$Z_{i,j} = \sum_{m=0}^{M-1} \sum_{n=0}^{N-1} X_{i+m,j+n} \times W_{m,n} + b \quad (3)$$

The resulting values undergo Rectified Linear Unit (ReLU) activation to introduce non-linearity, enhancing the model's capacity to capture complex patterns using equation (4) to the output values $Z_{i,j}$

$$ReLU(Z_{i,j}) = max(0, Z_{i,j}) \quad (4)$$

Batch normalization is employed to standardize inputs, stabilizing the training process by reducing internal covariate shifts. Additionally, max pooling is utilized to downsample feature maps, reducing spatial dimensions while retaining essential features, enhancing the model's robustness, and reducing computational complexity. By stacking these convolutional, batch normalization, and max pooling layers, the model can build a hierarchical representation of the input image, capturing increasingly complex visual patterns that are essential for the overall task of the model architecture.

Residual Blocks

The model incorporates residual blocks, which are a key component of modern CNN architectures. Residual blocks are essential architectural elements designed to address the challenges associated with training deep neural networks. Each residual block comprises two convolutional layers, each followed by batch normalization. Crucially, a skip connection is introduced, enabling the input of the block to be directly added to its output. This skip connection facilitates the flow of information during training and helps alleviate the vanishing gradient problem, ensuring effective training of deeper networks.

Inception Modules

Inception modules are specialized components aimed at capturing features at multiple scales within the network architecture. Each module consists of four parallel convolutional paths, each employing different kernel sizes (1x1, 3x3, 5x5), along with a max pooling layer. The outputs from these paths are concatenated, enabling the model to learn diverse feature representations. By leveraging multiple kernel sizes and pooling operations, inception modules enable the model to capture features

at different levels of granularity, thereby enhancing its ability to represent complex patterns in the input data.

Additional Convolutional Layers

Additional convolutional layers are introduced following residual blocks and inception modules to further refine feature extraction. These layers continue to apply convolution operations, followed by batch normalization and max pooling as needed. By building upon the hierarchical representations learned by earlier layers, additional convolutional layers enable the model to capture increasingly complex visual patterns present in the input data and prepare the features for integration with the GCN layers.

Graph Convolutional Layers

The key component that distinguishes the model from a traditional CNN is the inclusion of Graph Convolutional Layers. These layers take two inputs: the feature maps from the previous layers and an adjacency matrix (A) that represents the graph structure. Through matrix multiplications, these Graph Convolutional Layers facilitate the propagation of information across the graph, enabling the model to glean insights from both image data and the relational intricacies embedded within the graph. Let X denote the input feature matrix representing the node features, and A represents the adjacency matrix capturing the relationships between nodes in a graph. The GCN layer performs a convolutional operation on the graph data, which is mathematically expressed in equation (5).

$$Z = \sigma(A \cdot X \cdot W) \tag{5}$$

X is the input feature matrix of shape ($N \times D$), where N is the number of nodes and D is the number of features per node. A is the adjacency matrix of the graph, representing the relationships between nodes. It is typically normalized or pre-processed to capture the graph structure effectively. W is the learnable weight matrix of the GCN layer, which transforms the input features to a new feature space. It has dimensions ($D \times F$), where F is the number of output features or filters. σ represents the activation function applied element-wise to the output of the convolutional operation.

Output Layer

The final layer of the model is a dense layer with a sigmoid activation function, responsible for producing class predictions. Equation (6) explains the sigmoid activation function where z is the input to the activation function.

$$\sigma(z) = \frac{1}{1+e^{-z}} \tag{6}$$

The number of output units in this layer corresponds to the number of classes in the classification task. The sigmoid activation function scales the output values between 0 and 1, representing the model's confidence in each class. This layer produces the final output of the model, providing predictions for the input data based on the learned features and relationships captured throughout the network architecture.

4 Experimentations and Results

The dataset utilized by the authors comprises 15,000 histopathological images, each measuring 768 x 768 pixels and stored in JPEG format [26]. These images are categorized into three classes: lung adenocarcinoma, lung squamous cell carcinoma, and benign lung tissue. Initially sourced from HIPAA-compliant and validated repositories, the dataset originally contained 750 images of lung tissue, equally distributed among the three classes. Further, the dataset has been augmented using the Augmentor package, resulting in 15,000 images. Each class in the augmented dataset now consists of 5,000 images, ensuring a balanced distribution across the classes. Fig. 2 demonstrates the equal distribution of data classes in the dataset.

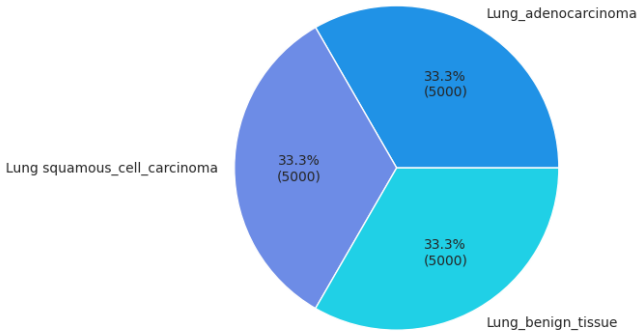

Fig. 2. Data Class Distribution

Histopathological images of lung adenocarcinoma typically exhibit irregularly shaped glandular structures, often characterized by varying degrees of differentiation and the presence of mucin production. Conversely, lung squamous cell carcinoma images commonly display keratinization and intercellular bridges, reflecting their origins from squamous epithelial cells. Fig. 3 gives the visual representation of the three classes of data utilized in the experimentations.

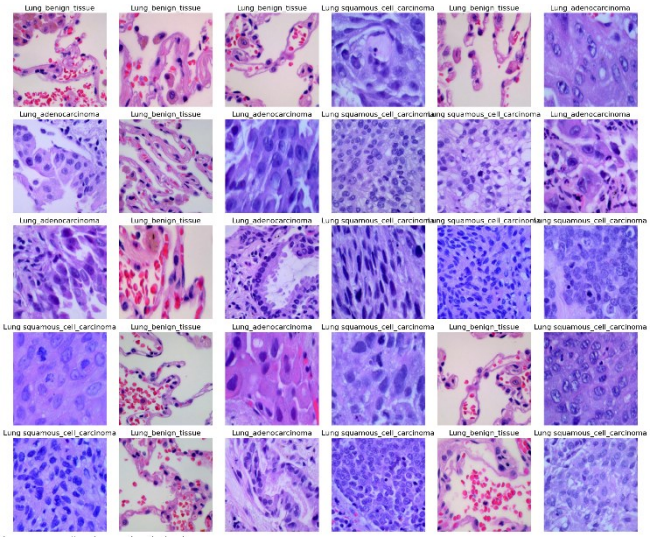

Fig. 3. Histopathological Image Variations Across Lung Tissue Classes

Benign lung tissue histopathological images, on the other hand, demonstrate a more uniform appearance with organized lung parenchyma, absence of atypical cellular features, and minimal architectural distortion. These distinctions arise from the diverse cellular origins and pathological characteristics associated with each type of lung tissue, facilitating their differentiation in histopathological analysis.

The model has been compiled using the Adamax optimizer with a learning rate set to 0.001. The choice of optimizer and learning rate affects how the model adjusts its weights during training to minimize the loss function. In the study, categorical cross-entropy is employed as the loss function. Categorical cross-entropy is particularly suitable for multi-class classification tasks like the one at hand, where the model needs to predict one class out of several mutually exclusive classes. It quantifies the difference between the predicted probability distribution and the true distribution of class labels. Additionally, accuracy is utilized as a primary evaluation metric to measure the model's classification performance on the validation and test datasets.

10

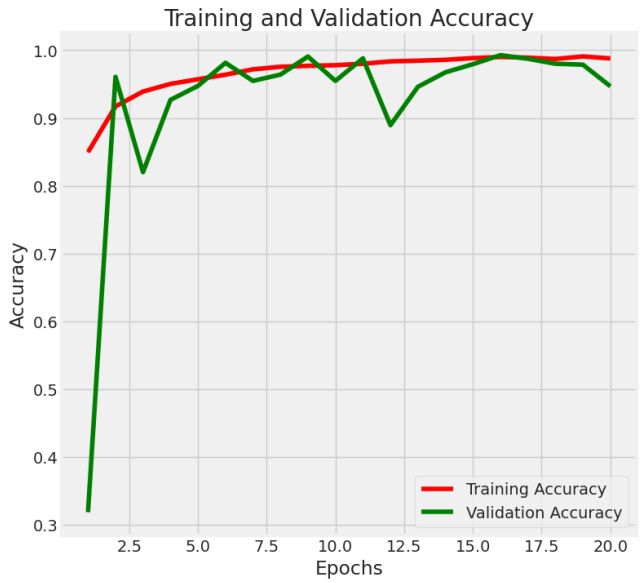

Fig. 4. Model Training and Validation Accuracy

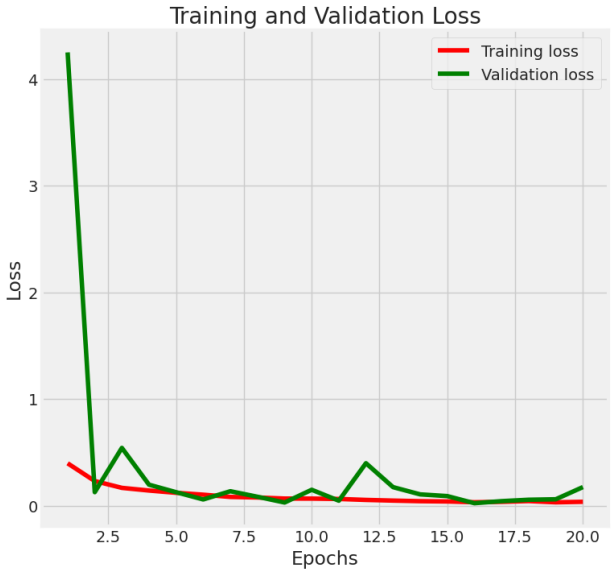

Fig. 5. Model Training and Validation Loss

The integration of convolutional neural network (CNN) and graph convolutional network (GCN) layers demonstrates cutting-edge performance in image classification tasks. After training the model on a dataset comprising 15,000 images

over 20 epochs, the achieved accuracy and loss metrics reflect the model's robustness. Notably, the training accuracy reaches 0.9610 with a corresponding loss of 0.1326, indicating the model's proficiency in learning from the training data. The test accuracy, evaluated on previously unseen data, is also high at 0.9520, with a test loss of 0.1770, demonstrating the model's ability to generalize well. Fig. 4 and Fig. 5 give the pictorial validation of the achieved results. Additionally, the validation accuracy stands at 0.9446, coupled with a validation loss of 0.1745, further validating the model's effectiveness and consistency in performance across different datasets. Table. 1 gives the evaluation metrics for each of the classes by calculating the values from the confusion matrix. The diagonal cells of the matrix represent the number of correct predictions (True Positives), while the off-diagonal cells show where the model is making mistakes (False Positives and False Negatives).

Table 1. Evaluation Metrics For Each Class

Class Name	Accuracy	Precision	Recall	F1-Score
Lung Squamous Cell Carcinoma	0.9662	0.9933	0.9026	0.9457
Lung Adenocarcinoma	0.9833	0.8799	0.9939	0.9334
Lung Benign Tissue	0.9846	0.9959	0.9590	0.9771
Average	**0.9780**	**0.9563**	**0.9518**	**95.20**

Accuracy measures the proportion of correctly classified instances out of the total instances. Precision measures the proportion of true positive predictions out of all positive predictions. Recall measures the proportion of true positive predictions out of all actual positive instances. F1 score is the harmonic mean of precision and recall, balancing both metrics.

$$\text{Accuracy} = \frac{TP+TN}{TP+TN+FN+FP} \tag{7}$$

$$\text{Precision} = \frac{TP}{TP+FP} \tag{8}$$

$$\text{Recall} = \frac{TP}{TP+FN} \tag{9}$$

$$\text{F1 Score} = \frac{2 \times Recall \times Precision}{Recall + Precision} \tag{10}$$

In equations (7), (8), (9), and (10), TP signifies true positive, TN signifies true negative, FP is false positive, and FN is false negative. The performance of the proposed CNN-GCN fused model has been meticulously compared with other state-of-the-art models and architectures. Table. II provides a comprehensive evaluation and thorough understanding of the proposed model's effectiveness with existing cutting-edge approaches in the field.

Table 1. Comparison of Proposed Model Performance Metrics

Model	Accuracy (%)
CNN - GCN (Our Model)	97.80
Alexnet CNN [10]	96.00
3D – CNN [13]	86.60
ANN [17]	96.67
MIL - GNN [20]	97.42
Multi-Path CNN [25]	87.80
RNN – GAN [27]	**98.60**
Deep Residual U-Net [28]	94.96
Attention-Based RNN [29]	97.47
Distanced LSTM [30]	89.05

Table. 2 presents a comparison of the accuracy achieved by the proposed CNN - GCN model with several state-of-the-art methods utilized in the field of lung cancer detection. Remarkably, our model outperforms most of the existing techniques, achieving an accuracy of 97.80%. Notably, the RNN-GAN model also demonstrates competitive performance with an accuracy of 98.60%. However, models such as the Multi-Path CNN and the Distanced LSTM exhibit comparatively lower accuracies of 87.80% and 89.05%, respectively. Due to several key factors, the proposed model showcases superior performance compared to other methods. Firstly, the combination of CNN and GCN allows our model to effectively capture both spatial features from histopathological images and relational information from the underlying graph structure, resulting in a more comprehensive representation of lung

cancer characteristics [31][32]. Additionally, by leveraging GCN, our model can exploit the interdependencies among data points within the graph, enhancing its ability to discern complex patterns and relationships crucial for accurate classification. This holistic approach enables our model to achieve higher accuracy rates, as evidenced by its superior performance compared to other state-of-the-art methods. Overall, the integration of CNN with GCN enhances the model's capacity to capture diverse and informative features, thereby facilitating more accurate and reliable detection of lung cancer.

5 Discussion and Conclusion

Based on the findings and results presented in the preceding sections, the performance metrics for each class of the dataset are meticulously analyzed and visually represented in Fig. 7. A detailed evaluation of the model performance may be given based on the presented performance criteria. Lung Squamous Cell Carcinoma shows slightly lower Precision and F1-Score compared to the other two conditions, which might suggest a need for further model refinement for this particular cancer type. In contrast, Lung Adenocarcinoma exhibits the highest Accuracy, but this does not translate to the highest scores in the other metrics, implying that while it is accurate, there may be room for improvement in its precision and recall balance. Lung Benign Tissue stands out with consistently high scores across all metrics, suggesting that the model is particularly adept at identifying benign cases with a high degree of confidence.

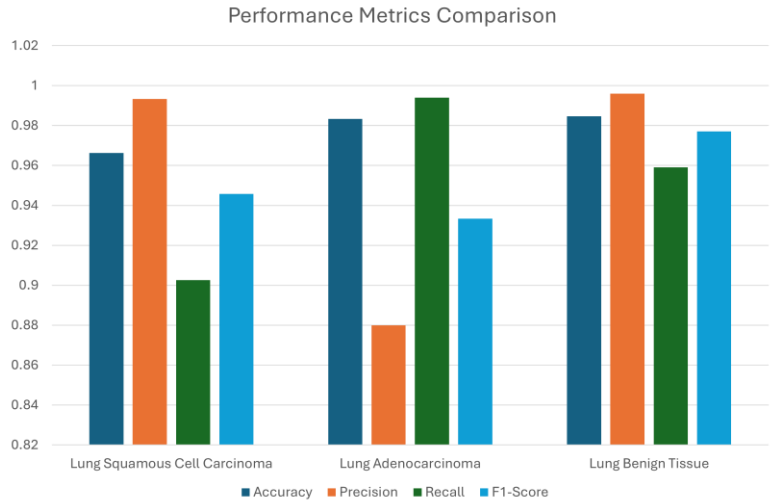

Fig. 7. Performance Metrics Comparison Chart

The high Recall scores for both cancer types indicate that the models are effective at identifying true positive cases, which is crucial in medical diagnostics to ensure that cases are not missed. Lastly, the uniformly high F1 scores across all conditions reflect a balanced performance between Precision and Recall, which is desirable in

a diagnostic tool as it ensures both the accuracy of the diagnosis and the minimization of false positives or negatives.

In conclusion, the study presents a novel approach integrating CNN with GCN for lung cancer detection. The proposed model achieves superior performance compared to state-of-the-art methods, with high accuracy and robust generalization to unseen data. Through comprehensive evaluation and analysis, the authors have demonstrated the effectiveness of the model in accurately detecting lung cancer subtypes. These findings underscore the potential of CNN-GCN fusion models in enhancing cancer detection accuracy and advancing medical diagnostics. In the future, there is substantial scope for enhancing and extending our work in several directions. Firstly, the integration of additional data modalities, such as genetic information or clinical data, could improve the model's predictive power and enable more personalized diagnostics and treatments. Additionally, exploring transfer learning techniques to leverage pre-trained models on larger datasets may further enhance model performance. Moreover, investigating the interpretability of the model's predictions could provide valuable insights into the underlying biological mechanisms of lung cancer. Lastly, deploying the developed model in real-world clinical settings and conducting prospective studies would validate its efficacy and pave the way for its adoption in clinical practice.

References

1. Wadowska, Katarzyna & Bil-Lula, Iwona & Trembecki, Łukasz & Sliwinska-Mosson, Mariola. (2020). Genetic Markers in Lung Cancer Diagnosis: A Review. International Journal of Molecular Sciences. 21. 4569.
2. W. Rahane, H. Dalvi, Y. Magar, A. Kalane and S. Jondhale, "Lung Cancer Detection Using Image Processing and Machine Learning HealthCare," *2018 International Conference on Current Trends towards Converging Technologies (ICCTCT)*, Coimbatore, India, 2018, pp. 1-5
3. A. Chaudhary and S. S. Singh, "Lung Cancer Detection on CT Images by Using Image Processing," *2012 International Conference on Computing Sciences*, Phagwara, India, 2012, pp. 142-146
4. Kale, Prajakta & Khadkikar, Prajakta. (2022). The International journal of analytical and experimental modal analysis Lung Cancer Prognosis by Implementing Various Evolutionary Image Processing Steps.
5. A. Thomas, A. Rajan, A. Lopez-Chavez, Y. Wang, G. Giaccone, From targets to targeted therapies and molecular profiling in non-small cell lung carcinoma, Annals of Oncology, Volume 24, Issue 3, 2013, Pages 577-585
6. Asuntha, A., Srinivasan, A. Deep learning for lung Cancer detection and classification. Multimed Tools Appl 79, 7731–7762 (2020).
7. S. Zheng *et al*., "Multi-Modal Graph Learning for Disease Prediction," in IEEE Transactions on Medical Imaging, vol. 41, no. 9, pp. 2207-2216, Sept. 2022.
8. Hou, W., Huang, H., Peng, Q., Yu, R., Yu, L., Wang, L. (2022). Spatial-Hierarchical Graph Neural Network with Dynamic Structure Learning for Histological Image Classification. In: Wang, L., Dou, Q., Fletcher, P.T., Speidel, S., Li, S. (eds) Medical Image Computing and Computer Assisted Intervention – MICCAI 2022. MICCAI 2022. Lecture Notes in Computer Science, vol 13432. Springer, Cham.
9. M. Adnan, S. Kalra and H. Tizhoosh, "Representation Learning of Histopathology Images using Graph Neural Networks," in 2020 IEEE/CVF Conference on Computer Vision and Pattern Recognition Workshops (CVPRW), Seattle, WA, USA, 2020 pp. 4254-4261.

10. A. Agarwal, K. Patni and R. D, "Lung Cancer Detection and Classification Based on Alexnet CNN," 2021 6th International Conference on Communication and Electronics Systems (ICCES), Coimbatre, India, 2021, pp. 1390-1397.
11. Sethy, Prabira Kumar et al. 'Lung Cancer Histopathological Image Classification Using Wavelets and AlexNet', vol. 31, Journal of X-Ray Science and technology 1 Jan. 2023 : 211 – 221
12. Yeguo Xu, Yuhang Wang, Navid Razmjooy,Lung cancer diagnosis in CT images based on Alexnet optimized by modified Bowerbird optimization algorithm, Biomedical Signal Processing and Control, Volume 77, 2022.
13. Wafaa Alakwaa, Mohammad Nassef and Amr Badr, "Lung Cancer Detection and Classification with 3D Convolutional Neural Network (3D-CNN)" International Journal of Advanced Computer Science and Applications(IJACSA), 8(8), 2017
14. Ahmed, T., Parvin, M.S., Haque, M.R. and Uddin, M.S. (2020) Lung Cancer Detection Using CT Image Based on 3D Convolutional Neural Network. Journal of Computer and Communications, 8, 35-42.
15. T. Jin, H. Cui, S. Zeng and X. Wang, "Learning Deep Spatial Lung Features by 3D Convolutional Neural Network for Early Cancer Detection," *2017 International Conference on Digital Image Computing: Techniques and Applications (DICTA)*, Sydney, NSW, Australia, 2017, pp. 1-6.
16. Eali Stephen Neal Joshua, Debnath Bhattacharyya, Midhun Chakkravarthy, Yung-Cheol Byun, "3D CNN with Visual Insights for Early Detection of Lung Cancer Using Gradient-Weighted Class Activation", Journal of Healthcare Engineering, vol. 2021, Article ID 6695518, 11 pages, 2021.
17. Nasser, Ibrahim M. and Abu-Naser, Samy S., Lung Cancer Detection Using Artificial Neural Network (March 2019). International Journal of Engineering and Information Systems (IJEAIS), 3(3), 17-23, March 2019.
18. Zhi-Hua Zhou, Yuan Jiang, Yu-Bin Yang, Shi-Fu Chen, Lung cancer cell identification based on artificial neural network ensembles, Artificial Intelligence in Medicine, Volume 24, Issue 1, 2002, Pages 25-36.
19. Lian, Jie & Long, Yonghao & Huang, Fan & Ng, Douglas & Lee, Faith & Lam, David & Fang, Benjamin X & Dou, Qi & Vardhanabhuti, Vince. (2022). Imaging-Based Deep Graph Neural Networks for Survival Analysis in Early Stage Lung Cancer Using CT: A Multicenter Study. Frontiers in Oncology.
20. Aftab, R., Qiang, Y., Zhao, J. et al. Graph Neural Network for representation learning of lung cancer. BMC Cancer 23, 1037 (2023).
21. Zhi, Hong-Yi & Zhao, Lu & Lee, Chun-Cheng & Chen, Chen. (2021). A Novel Graph Neural Network Methodology to Investigate Dihydroorotate Dehydrogenase Inhibitors in Small Cell Lung Cancer. Biomolecules. 11. 477.
22. S. Das and S. Majumder, "Lung Cancer Detection Using Deep Learning Network: A Comparative Analysis," 2020 Fifth International Conference on Research in Computational Intelligence and Communication Networks (ICRCICN), Bangalore, India, 2020, pp. 30-35
23. F. Taher and R. Sammouda, "Lung cancer detection by using artificial neural network and fuzzy clustering methods," *2011 IEEE GCC Conference and Exhibition (GCC)*, Dubai, United Arab Emirates, 2011, pp. 295-298
24. S.R. Kannan, R. Devi, S. Ramathilagam, T.-P. Hong, A. Ravikumar, Robust fuzzy clustering algorithms in analyzing high-dimensional cancer databases, Applied Soft Computing, Volume 35, 2015, Pages 199-213.
25. Sori, W.J., Feng, J. & Liu, S. Multi-path convolutional neural network for lung cancer detection. Multidim Syst Sign Process 30, 1749–1768 (2019).
26. Borkowski AA, Bui MM, Thomas LB, Wilson CP, DeLand LA, Mastorides SM. Lung and Colon Cancer Histopathological Image Dataset (LC25000). arXiv:1912.12142v1 [eess.IV], 2019

27. Atul Tiwari, Shaikh Abdul Hannan, Rajasekhar Pinnamaneni, Abdul Rahman Mohammed Al-Ansari, Yousef A.Baker El-Ebiary, S. Prema and R. Manikandan, "Optimized Ensemble of Hybrid RNN-GAN Models for Accurate and Automated Lung Tumour Detection from CT Images" International Journal of Advanced Computer Science and Applications(IJACSA), 14(7), 2023.
28. Mishra, Vaibhav. (2023). "Deep Residual Custom U-Net for Enhanced Lung Image Segmentation: A ResNet152 Encoder Approach".
29. S. Sasikumar, P. N. Renjith, K. Ramesh and K. S. Sankaran, "Attention Based Recurrent Neural Network for Lung Cancer Detection," *2020 Fourth International Conference on I-SMAC (IoT in Social, Mobile,* Analytics and Cloud) (I-SMAC), Palladam, India, 2020, pp. 720-724.
30. Gao, R. et al. (2019). Distanced LSTM: Time-Distanced Gates in Long Short-Term Memory Models for Lung Cancer Detection. In: Suk, HI., Liu, M., Yan, P., Lian, C. (eds) Machine Learning in Medical Imaging. MLMI 2019. Lecture Notes in Computer Science(), vol 11861. Springer, Cham.
31. M. Goswami, N. Panda, S. Mohanty and P. K. Pattnaik, "Machine Learning Techniques and Routing Protocols in 5G and 6G Mobile Network Communication System - An Overview," *2023 7th* International Conference on Trends in Electronics and Informatics (ICOEI), Tirunelveli, India, 2023, pp. 1094-1101
32. Q. Liu, L. Xiao, J. Yang and Z. Wei, "CNN-Enhanced Graph Convolutional Network With Pixel- and Superpixel-Level Feature Fusion for Hyperspectral Image Classification," in *IEEE Transactions on Geoscience and Remote Sensing*, vol. 59, no. 10, pp. 8657-8671, Oct. 2021